Enhancement of mechanical and thermoelectric properties of $Ca_3Co_4O_9$ by Ag addition

F. Kahraman[1], M. A. Madre[2], Sh. Rasekh[2], C. Salvador[2], P. Bosque[3], M. A. Torres[2], J. C. Diez[2], A. Sotelo[2]

[1]Tarsus Technology Faculty, Mersin University,33400,Tarsus-Mersin,Turkey

[2] ICMA (Universidad de Zaragoza-CSIC), Dpto. de Ciencia y Tecnología de Materiales y Fluidos, C/María de Luna 3, E-50018-Zaragoza, Spain

[3] Centro Universitario de la Defensa de Zaragoza. Academia General Militar. Ctra. de Huesca s/n. 50090-Zaragoza, Spain

Abstract

$Ca_3Co_4O_9$ + x wt% Ag (x=0, 1, 3, 5, and 10) polycrystalline thermoelectric ceramics have been prepared by a sol-gel route via nitrates followed by high temperature treatment before sintering. Out-of-plane XRD data have shown that major phase is the $Ca_3Co_4O_9$ one, accompanied by metallic Ag. SEM observations have agreed with the XRD data. Apparent density measurements have revealed that all samples possess densities ranging between 80 and 90 % when Ag content is raised. Mechanical properties have shown a drastic increase of bending stress when Ag is added to the samples. Electrical resistivity decreases with the Ag content, compared with the pure ones, while Seebeck coefficient slightly decreases. Maximum power factor values around 0.43 mW/K^2m at 800 ºC have been achieved for the 10 wt% Ag samples which is much higher than the measured in the pure $Ca_3Co_4O_9$ samples.

Keywords: $Ca_3Co_4O_9$, flexural strength, thermoelectricity

Corresponding author: Funda Kahraman

e-mail: kahraman.funda@yahoo.com.tr

Address: Tarsus Technology Faculty, Mersin University,33400,Tarsus-Mersin,Turkey

Tel: +905372741556

Fax: +903246274805

1. Introduction

Thermoelectric (TE) materials possess the ability to directly transform, without any mobile element, a temperature difference to electrical power due to the Seebeck effect. The efficiency of these materials is quantified by a dimensionless coefficient known as the figure-of-merit, ZT. This parameter is defined as $TS^2/\rho\kappa$ (in which S^2/ρ is also called power factor, PF), where S, ρ, κ, and T are Seebeck coefficient, electrical resistivity, thermal conductivity, and absolute temperature, respectively [1]. Nowadays, these materials are attracting a high interest to be used in several applications as waste heat recovery devices [2] or solar thermoelectric generators [3]. In these systems, TE materials can increase their global efficiency, reducing the amount of fossil fuels and, consequently, the release of greenhouse gasses, helping to fight against global warming. Furthermore, they can also be used as heating/refrigeration devices avoiding the use of harmful gases [4].

At present, the practical applications of TE devices are limited to materials displaying high ZT values at working temperatures, as some intermetallic ones, such as Bi_2Te_3, or PbTe with high ZT at relatively low temperatures [5-7]. As a consequence, these systems are involved in low power refrigeration or heat harvesting in relatively low temperature environments, e.g. in vehicles exhaust. However, due to their degradation under air at high working temperatures, they cannot be applied in devices working in such conditions. Due to these temperature limitations, some of the most important sources of wasted heat (for example, thermal power stations) cannot be used. These temperature limitations were overcome by the discovery of attractive thermoelectric properties in $Na_2Co_2O_4$ ceramics [8], composed of cheaper, more abundant,

and environmentally friendly elements than the intermetallic ones [9]. Since the discovery of this thermoelectric oxide, much work has been performed on the cobalt-based ceramics as promising thermoelectric materials for high temperature applications. The intense research work devoted on those ceramics led to the discovery and optimization of new compositions, such as $Ca_3Co_4O_9$, $Bi_2Sr_2Co_2O_x$, $Bi_2Ca_2Co_2O_x$, and $Bi_2Ba_2Co_2O_x$ with interesting thermoelectric properties and high working temperatures [10,16]. Crystallographic studies performed on those Co-based materials have demonstrated that they can be described using a monoclinic structure. On the other hand, this structure is composed by the alternate stacking of two different layers, a common conductive CdI_2-type hexagonal CoO_2 layer with a two-dimensional triangular lattice and a block layer composed of insulating rock-salt-type (RS) layers. The two sublattices (RS block and CdI_2-type CoO_2 layer) possess common a- and c-axis lattice parameters and β angles, but different b-axis length, causing a misfit along the b-direction [17-19]. The preferential growth habit through the ab plane in these materials leads to the formation of plate-like grains during the crystallisation process. This shape anisotropy opens the route to preferentially align the grains along the conducting planes which could help reaching TE properties comparable to those obtained on single crystals. Numerous methods have been reported to be efficient to produce well aligned grains, in these or in similar anisotropic systems, such as hot uniaxial pressing [20], templated grain growth (TGG) [19], spark plasma sintering [21], laser floating zone melting (LFZ) [22], electrically assisted laser floating zone [23], *etc*. On the other hand, these methods possess some drawbacks due to different factors, as the relatively long treatments required for the first two ones,

or the high costs associated with the equipment and the strong dependence of thermoelectric properties on the growth or the texturing speeds for the other ones [19,21,24,25].

Another possibility arising from the crystal structure of these materials has been put in evidence in some studies reporting that the Seebeck coefficient values are governed by the incommensurability ratio and/or the charge of the RS block layer between the CoO_2 ones [26]. This characteristic provides the basis for the modification of thermoelectric properties of a given material via chemical substitutions. The most common ones substitute Ca or Co in $Ca_3Co_4O_9$ [27-29], or Bi or the alkaline earth (AE) in $Bi_2AE_2Co_2O_x$ [30-32]. Moreover, it has also been demonstrated that metallic Ag additions in these or similar systems are adequate to promote higher mechanical and electrical properties [33-36].

The aim of this work is to study the effect of Ag additions in different weight % proportions to $Ca_3Co_4O_9$ samples, on the microstructural, electric and thermoelectric characteristics of relatively high-density sintered bulk materials prepared by a sol-gel synthesis route.

2. Experimental

$Ca_3Co_4O_9$ + x wt.% Ag polycrystalline ceramic materials, with x = 0, 1, 3, 5, and 10 were prepared by a sol-gel route using commercial $CaCO_3$ (≥ 99%, Aldrich), $Co(NO_3)_2 \cdot 6H_2O$ (≥ 99%, Aldrich), and Ag (99.9 %, Aldrich) powders as starting materials. They were weighed in the appropriate proportions and dissolved in a mixture of distilled water and HNO_3 (analysis grade, Panreac). To the resulting clear pink solution citric acid (99.5 %, Panreac), and ethylene glycol (99 %, Panreac) were added in the adequate proportions. Evaporation of the solvent

was slowly performed in order to decompose the nitric acid excess, which allows the polymerization reaction between ethylene glycol and citric acid, producing a pink gel where the cations are coordinated [37]. The dried product was then decomposed (slow self combustion) by heating at 450 ºC for 1 h. The resulting powder was thermally treated twice, at 750 and 800 ºC for 12 h each one, with an intermediate milling, to assure the complete calcium carbonate decomposition. After thermal treatments, the powders were uniaxially pressed at 400 MPa for 1 minute to obtain green tetragonal ceramic bodies (~ 3 mm x 3 mm x 25 mm), with an adequate size and shape for their mechanical and thermoelectric characterization. In order to produce high density materials, the sintering procedure has been performed following a previously developed process consisting in a thermal treatment, under air atmosphere, at 1200 ºC for 12 h, followed by 900 ºC for 24 h [38] with a final furnace cooling. The first step promotes high densification as it is relatively close to the melting point of this system while the second one promotes the formation of $Ca_3Co_4O_9$ phase [39]. Out-of-plane X-ray diffraction (XRD) patterns performed on the samples surfaces have been systematically recorded in order to identify the different phases in the thermoelectric sintered materials. Data have been collected at room temperature, with 2θ ranging between 5 and 60 degrees, using a Rigaku D/max-B X-ray powder diffractometer working with Cu Kα radiation. Microstructural observations were performed on longitudinal surfaces and polished sections, and on transversal fractured surfaces of the samples, using a Field Emission Scanning Electron Microscope (FESEM, Carl Zeiss Merlin) fitted with an energy dispersive spectrometry (EDS) device. Several representative micrographs have been used to analyze the different phases content and their

distribution. Moreover, apparent density measurements have been performed on several samples for each composition after sintering, using 4.677 g/cm^3 as $Ca_3Co_4O_9$ theoretical density [40] and 10.5 g/cm^3 as Ag theoretical one [41]. Oxygen content was determined in all the samples using cerimetric titrations, following the procedure described elsewhere [40]. Mechanical characterization has been performed by flexural strength (σ_{max}), using the three-point bending test in an Instron 5565 machine, at 30 μm/min, with a 15 mm loading span fixture. Electrical resistivity and Seebeck coefficient were simultaneously determined by the standard dc four-probe technique in a LSR-3 measurement system (Linseis GmbH), in the steady state mode and at temperatures ranging from 50 to 800 ºC under He atmosphere. With the electrical resistivity and Seebeck coefficient data, the power factor has been calculated in order to determine the samples performances. These properties have been compared with the results obtained in the undoped samples prepared in this work and with those reported in the literature at room temperature (~ 50 ºC), where oxygen diffusion is negligible, to avoid the influence of the atmosphere on the compared values.

3. Results and discussion

Out-of-plane XRD patterns for the $Ca_3Co_4O_9$ + xwt.% Ag samples are displayed in Fig. 1 (from 10 to 40º for clarity). These plots show the evolution of the samples with Ag doping, indicating that all the samples have practically the same diffraction patterns except for the Ag peak. In all samples the highest peaks are associated to the thermoelectric $Ca_3Co_4O_9$ phase, indicated by the reflection planes in Fig. 1e, in agreement with previously reported data [42]. In

this figure, it has also been indicated the peak at around 38.2 degrees (#) which corresponds to the (111) diffraction plane of Ag [43]. The presence of only $Ca_3Co_4O_9$ phase and Ag in the final samples is a good indication that the two-steps sintering process has been successful, taking into account that the first temperature (1200 ºC) is higher than the $Ca_3Co_4O_9$ phase maximum stability temperature (around 925 ºC) [39], producing the $Ca_3Co_4O_9$ decomposition into CaO(CoO) and CoO(CaO) solid solutions [40]. Moreover, it is also higher than the Ag melting temperature (960 ºC) [41] which could produce liquid Ag losses. After sintering procedure, no Ag has been found to be outside the bulk samples. As a consequence, it can be deduced that molten Ag has produced a liquid phase inside the bulk material, increasing the diffusion speed, but solidifying inside the bulk samples when the temperature is decreased to 900 ºC for the second sintering step. On the other hand, in order to determine if Ag is incorporated in the crystal structure, cell parameters and volumes have been calculated using fullprof software using a C2/m space group and displayed in Table I. As it can be easily observed in the table, only slight differences can be found in the cell parameters, leading to nearly unchanged cell volumes in all cases. As a consequence, it can be deduced that no Ag has been incorporated in the $Ca_3Co_4O_9$ cell.

SEM micrographs performed on representative longitudinal polished sections of samples are presented in Fig. 2. In the figure, it can be clearly seen that all samples are composed by the thermoelectric $Ca_3Co_4O_y$ one (grey contrast) and metallic Ag (white contrast), indicated by arrows in Fig. 2b. In the micrographs it can be observed that Ag grains amount is raised with the nominal Ag content. All these observations are in clear agreement with the XRD data discussed

previously. Moreover, when observing the higher magnification micrograph shown in Fig. 2f, it can be seen that Ag is found in the intergranular regions, filling the holes between TE grains. This situation has been demonstrated to be very favorable in other ceramic systems to enhance the electrical and mechanical properties of the bulk materials [36,44] and, as a consequence, it is expected the same effect in this system.

In order to better know the reasons why liquid Ag has been kept inside the bulk materials, their surfaces have been studied by SEM microscopy and the representative images for all the samples are displayed in Fig. 3. In these images it is clear that major contrast is the grey one, associated by EDS to the $Ca_3Co_4O_9$ phase. Moreover, at this magnification Ag is not observed in the surface, indicating that liquid Ag migration at high temperatures to the surfaces has not been produced. This effect is probably due to the fact that Ag has been very well distributed as small particles all along the bulk samples, which is the typical effect of the sol-gel synthesis method. Furthermore, the high densification obtained in these samples leads to relatively low porosity (see black contrast in Fig. 3) and, consequently, closes the routes for Ag to reach the external bulk surfaces. On the other hand, from the surface images, it is not clear to assess which is the density evolution of these samples with the Ag content. In order to clarify this evolution, apparent density measurements have been performed in all samples. The obtained results, together with their standard error and the % of the theoretical density, are displayed in Table II. From these data, it can be deduced that the performed thermal treatment is successful to obtain high density bulk $Ca_3Co_4O_9$ materials, in agreement with previous works [38]. Moreover, Ag additions increases in an important manner

the final density of the bulk materials due to the formation of a well distributed liquid phase which improves cations diffusion and, consequently, decreases porosity. On the other hand, this reduction in porosity is not enough to hinder oxygen diffusion inside the samples, avoiding the rapid formation of the $Ca_3Co_4O_9$ phase [40].

The flexural strength of the samples, together with their standard error, as a function of Ag content is presented in Fig. 4. From the figure, it is clear that Ag addition drastically enhances the flexural strength of samples in more than a factor two, compared with the pure $Ca_3Co_4O_9$ ones. Moreover, the raise in Ag contents also increases the σ_{max} values reaching a maximum of about 110 MPa for the 10 wt.% Ag. This effect is due to the presence of metallic Ag filling the intergranular spaces that appear in the thermoelectric matrix, providing a plastic-flow region which may resist crack propagation, as observed in similar systems [45].

The temperature dependence of electrical resistivity, as a function of Ag content, is shown in Fig. 5. The ρ (T) curves show a decrease of resistivity when Ag is added, compared with the undoped samples. The curves show a semiconducting-like ($d\rho/dT < 0$) behaviour in the whole measured temperature range. In all the samples with Ag additions, room temperature resistivity values decrease significantly. The electrical resistivity evolution can be explained by the presence of Ag in the samples, together with the raise in the bulk density when Ag content is increased, in agreement with the XRD data, SEM observations, and apparent density evolution discussed previously. The lowest measured room temperature resistivity values (~ 12 mΩ.cm for the 10 wt.% Ag samples) is much lower than the obtained in the pure $Ca_3Co_4O_9$ samples (about

31 mΩ.cm). On the other hand, they are higher than the obtained in similar samples produced by a more complex method followed by hot pressing (around 6, 5, and 3 mΩ.cm for the 0, 5, and 10 wt% Ag, respectively) and measured perpendicular to the pressing direction [35]. The lowest value at 800 ºC (~ 10 mΩ.cm for the 10 wt.% Ag samples) is still higher than the values measured in hot pressed samples with 0, 5, and 10 vol.% Ag at the same temperature (about 9, 5, and 2 mΩ.cm, respectively) and measured perpendicular to the pressing direction [46].

Fig. 6 shows the variation of the Seebeck coefficient with the temperature, as a function of Ag addition. In the plot, it can be clearly seen that the sign of the Seebeck coefficient is positive for the entire measured temperature range, which confirms a conduction mechanism mainly governed by holes. The Seebeck coefficient increases with temperature, with a similar trend for all the samples. On the other hand, S values decrease with Ag content, in agreement with the evolution of their electrical resistivities. The maximum Seebeck coefficient at 50 ºC (~ room temperature), 135 μV/K has been obtained in samples with 0 and 1 wt.% Ag, slightly decreasing when the Ag content is raised. These values are the same as the obtained in previous works at the same temperature in sintered materials (~ 135 μV/K) [11], but much lower than the obtained in laser floating zone textured ones (~ 170 μV/K) [40]. The differences in S values obtained in these works can be associated to modifications in the $Ca_3Co_4O_9$ oxygen content. As a consequence, in order to confirm this fact, the oxygen content in the samples prepared in this work has been evaluated by cerimetric titrations. The obtained values, in all cases have been a mean Co valence of 3.15 with a standard error of ± 0.01. On the other

hand, the Seebeck coefficient values obtained in this work at 800 ºC also decrease with the Ag content. Moreover, the maximum value at this temperature (~ 240 μV/K for the pure $Ca_3Co_4O_9$ samples) are significantly higher than the best values obtained for Ag added $Ca_3Co_4O_9$ samples consolidated by hot pressing (around 200 μV/K) [35,46].

In order to evaluate the thermoelectric performances of these materials, the power factor has been calculated using the ρ and S data, and plotted in Fig. 7. When considering PF values at around 50 ºC (~ room temperature), it can be clearly seen that all the samples with Ag possess higher PF values than the undoped ones. As it can be observed in the figure, PF values at this temperature are increased with Ag content until they reach the maximum values (~ 0.11 $mW/K^2.m$) for 10 wt.% Ag which is about 60 % higher than the obtained for the undoped samples. The highest PF value obtained in these samples is reached at 800 ºC (around 0.43 $mW/K^2.m$) for the 10 wt % Ag samples and is about 40 % higher than the obtained for the undoped samples. On the other hand, this value is approximately the same obtained in hot pressed samples with 7.5 vol.% Ag [46], but lower than the measured in 10 wt.% Ag added samples prepared by a more complex method followed by hot pressing (about 1 $mW/K^2.m$) [35]. In spite of these results, all the obtained data in this work clearly show that Ag additions in $Ca_3Co_4O_9$ ceramics can be used to produce high performance TE materials with randomly oriented grains by a simple, rapid, and economic route.

4. Conclusions

This paper demonstrates that Ag additions to $Ca_3Co_4O_9$ samples can be prepared by a two step sintering method. XRD data and SEM observations have shown that all samples are composed by the $Ca_3Co_4O_9$ phase, accompanied by metallic Ag. Moreover, Ag addition raises the samples density, due to the formation of a liquid phase which improves sinterability. The higher density, together with the presence of Ag filling the intergranular holes, drastically increases mechanical properties and decreases electrical resistivity in an important manner. On the other hand, S coefficient slightly decreases with the Ag content. In spite of this reduction, the maximum PF at 800 ºC of around 0.43 $mW/K^2.m$ has been obtained in the 10 wt.% Ag samples. These values are among the highest obtained in the $Ca_3Co_4O_9$ system reported in the literature, but produced by more complex, long, and expensive techniques. As a consequence, the method and doping used in this work could easily produce high performance TE materials for practical applications.

Acknowledgements

This research has been supported by the Spanish MINECO-FEDER (MAT2013-46505-C3-1-R). The authors wish to thank the Gobierno de Aragón-Fondo Social Europeo (Consolidated Research Groups T12 and T87) for financial support. The technical contributions of C. Estepa, and C. Gallego are also acknowledged. F. Kahraman acknowledges a financial grant from the Council of Higher Education (YÖK) in Turkey for international mobility

References

[1] Rowe DM. Thermoelectrics Handbook: Macro to Nano. first ed. Boca Raton:CRC Press;2006.

[2] Mahan G, Sales B, Sharp J, Thermoelectric materials: new approaches to an old problem. Phys Today 1997;50 (3):42–7.

[3] Naito H, Kohsaka Y, Cooke D, Arashi H. Development of a solar receiver for a high-efficiency thermionic/thermoelectric conversion system. Sol Energy 1996;58 (4-6):191–5.

[4] Elsheikh M H, Shnawah DA, Sabri MFM, Said SBM, Hassan MH, Bashir M BA, Mohamad M. A review on thermoelectric renewable energy: Principle parameters that affect their performance. Renew Sust Energ Rev 2014;30:337-55.

[5] Santamaria JM, Alkorta J, Sevillano JG. Mechanical properties of bismuth telluride (Bi_2Te_3) processed by high pressure torsion (HPT). Bol Soc Esp Ceram V 2013;52:137-42.

[6] Wang HC, Bahk J-H, Kang C, Hwang J, Kim K, Kim J, Burke P, Bowers JE, Gossard AC, Shakouri A, Kim W. Right sizes of nano- and microstructures for high-performance and rigid bulk thermoelectrics. P Natl Acad Sci USA 2014;111:10949-54.

[7] Wang HC, Hwang J, Snedaker ML, Kim I-H, Kang C, Kim J, Stucky GD, Bowers J, Kim W. High Thermoelectric Performance of a Heterogeneous PbTe Nanocomposite. Chem Mater 2015;27:944-9.

[8] Terasaki I, Sasago Y, Uchinokura K. Large thermoelectric power in $NaCo_2O_4$ single crystals. Phys Rev B 1997;56 (20):12685–7.

[9] Yaroshevsky AA. Abundances of chemical elements in the Earth's crust. Geochem Int 2006;44:48-55.

[10] Huang Y, Zhao B, Fang J, Ang R, Sun Y. Tunning of microstructure and thermoelectric properties of $Ca_3Co_4O_9$ ceramics by high-magnetic-field sintering. J Appl Phys 2011;110 (12):123713.

[11] Sotelo A, Constantinescu G, Rasekh Sh, Torres MA, Diez JC, Madre MA. Improvement of thermoelectric properties of $Ca_3Co_4O_9$ using soft chemistry synthetic methods. J Eur Ceram Soc 2012;32 (10):2415–22.

[12] Shen JJ, Liu XX, Zhu TJ, Zhao XB. Improved thermoelectric properties of La-doped $Bi_2Sr_2Co_2O_9$-layered misfit oxides. J Mater Sci 2009;44 (7):1889–93.

[13] Diez JC, Guilmeau E, Madre MA, Marinel S, Lemmonier S, Sotelo A, Improvement of $Bi_2Sr_2Co_{1.8}O_x$ thermoelectric properties by laser floating zone texturing. Solid State Ionics 2009;180 (11-13):827–30.

[14] Rubesova K, Hlasek T, Jakes V, Huber S, Hejtmanek J, Sedmidubsky D. Effect of a powder compaction process on the thermoelectric properties of $Bi_2Sr_2Co_{1.8}O_x$ ceramics. J Eur Ceram Soc 2015;35:525-31.

[15] X. G. Luo, Y. C. Jing, H. Chen, X. H. Chen, Intergrowth and thermoelectric properties in the Bi-Ca-Co-O system. J Crystal Growth 2007;308 (2):309–313.

[16] Ang R, Sun YP, Luo X, Song WH. A narrow band contribution with Anderson localization in Ag-doped layered cobaltites $Bi_2Ba_3Co_2O_y$. J Appl Phys 2007;102 (7):073721.

[17] Miyazaki Y. Crystal structure and thermoelectric properties of the misfit-layered cobalt oxides. Solid State Ionics 2004;172 (1-4):463–7.

[18] Maignan A, Hébert S, Hervieu M, Michel C, Pelloquin D, Khomskii D, Magnetoresistance and magnetothermopower properties of Bi/Ca/Co/O and

Bi(Pb)/Ca/Co/O misfit layer cobaltites. J Phys: Condens Matter 2003;15:2711-23.

[19] Itahara H, Xia C, Sugiyama J, Tani T. Fabrication of textured thermoelectric layered cobaltites with various rock salt-type layers by using β-$Co(OH)_2$ platelets as reactive templates. J Mater Chem 2004;14:61-6.

[20] Wang H, Sun X, Yan X, Huo D, Li X, Li J-G, Ding X. Fabrication and thermoelectric properties of highly textured $Ca_9Co_{12}O_{28}$ ceramic. J Alloys Compd 2014;582:294-8.

[21] Wu NY, Holgate TC, Nong NV, Pryds N, Linderoth S. High temperature thermoelectric properties of $Ca_3Co_4O_{9+\delta}$ by auto-combustion synthesis and spark plasma sintering. J Eur Ceram Soc 2014;34:925-31.

[22] Sotelo A, Rasekh Sh, Guilmeau E, Madre MA, Torres MA, Marinel S, Diez JC, Improved thermoelectric properties in directionally grown $Bi_2Sr_2Co_{1.8}O_y$ ceramics by Pb for Bi substitution. Mater Res Bull 2011;46 (12):2537–42.

[23] Ferreira NM, Rasekh Sh, Costa FM, Madre MA, Sotelo A, Diez JC,Torres M.A. New method to improve the grain alignment and performance of thermoelectric ceramics. Mater Lett 2012;83 :144–7.

[24] Rasekh Sh, Constantinescu G, Torres MA, Madre MA, Diez JC, Sotelo A. Growth rate effect on microstructure and thermoelectric properties of melt grown $Bi_2Ba_2Co_2O_x$ textured ceramics. Adv Appl Ceram 2012;111 (5):490–4.

[25] Constantinescu G, Rasekh Sh, Torres MA, Madre MA, Diez JC, Sotelo A. Enhancement of the high-temperature thermoelectric performance of $Bi_2Ba_2Co_2O_x$ ceramics. Scr Mater 2013;68(1):75–8.

[26] Maignan A, Pelloquin D, Hébert S, Klein Y, Hervieu M.Thermoelectric power in misfit cobaltites ceramics: optimization by chemical substitutions. B Soc Esp Ceram V 2006;45 (3):122–5.

[27] Demirel S, Aksan MA, Altin S. Low temperature electrical and thermal transport properties of the $Ca_{3-x}Sb_xCo_4O_9$ system. J Mater Sci: Mater Electron 2012;23 (12):2251–6.

[28] Diez JC, Torres MA, Rasekh Sh, Constantinescu G, Madre MA, Sotelo A. Enhancement of $Ca_3Co_4O_9$ thermoelectric properties by Cr for Co substitution. Ceram Int 2013;39 (6):6051–6.

[29] Abdellahi M, Bahmanpour M, Bahmanpour M. Modeling Seebeck coefficient of $Ca_{3-x}M_xCo_4O_9$ (M=Sr, Pr,Ga,Ca,Ba,La,Ag) thermoelectric ceramics. Ceram Int 2015;41:345-52.

[30] Madre MA, Torres MA, Rasekh Sh, Diez JC, Sotelo A. Improvement of thermoelectric performances of $Bi_2Sr_2Co_{1.8}O_x$ textured materials by Pb addition using a polymer solution method. Mater Lett 2012;76:5–7.

[31] Sun N, Dong ST, Zhang BB, Chen YB, Zhou J, Zhang ST, Gu ZB, Yao SH, Chen YF. Intrinsically modified thermoelectric performance of alkaline-earth isovalently substituted $[Bi_2AE_2O_4][CoO_2]_y$ single crystals. J Appl Phys 2013;114 (4):043705.

[32] Rasekh Sh, Madre MA, Diez JC, Guilmeau E, Marinel S, Sotelo, A. Effect of Pb substitution on the thermoelectrical properties of textured $Bi_2Ca_2Co_{1.7}O_y$ ceramics prepared by a polymer solution method. Bol Soc Esp Ceram V 2010;49:371-6.

[33] Zhang FP, Zhang X, Lu QM, Zhang JX, Liu YQ, Zhang GZ. Preparation and high temperature thermoelectric properties of $Ca_{3-x}Ag_xCo_4O_{9+\delta}$ oxides. Solid State Ionics 2011;201 (1):1–5.

[34] Ozkurt B, Madre MA, Sotelo A, Yakinci ME, Ozcelik B. Relationship Between Growth Speed, Microstructure, Mechanical and Electrical Properties in Bi-2212/Ag Textured Composites. J Supercond Nov Magn 2012;25:799-804.

[35] Mikami M, Ando N, Funahashi R. The effect of Ag addition on electrical properties of the thermoelectric compound $Ca_3Co_4O_9$. J Solid State Chem 2005;178:2186-90.

[36] Sotelo A, Torres MA, Constantinescu G, Rasekh Sh, Diez JC, Madre MA. Effect of Ag addition on the mechanical and thermoelectric performances of annealed $Bi_2Sr_2Co_{1.8}O_x$ textured ceramics. J Eur Ceram Soc 2012;32 (14):3745–51.

[37] Gaoke Z, Ying L, Xia Y, Yanping W, Shixi O, Hangxing L. Comparison of synthesis methods, crystal structure and characterization of strontium cobaltite powders. Mater Chem Phys 2006;99:88–95.

[38] Kang M-G, Cho K-H, Kim J-S, Nahm S, Yoon S-J, Kang C-Y. Post-calcination, a novel method to synthesize cobalt oxide-based thermoelectric materials. Acta Mater 2014;73:251-8.

[39] Sedmidubsky D, Jakes V, Jankovsky O, Leitner J, Sofer Z, Hejtmanek J. Phase equilibria in Ca–Co–O system. J Solid State Chem 2012;194:199–205.

[40] Madre MA, Costa FM, Ferreira NM, Sotelo A, Torres MA, Constantinescu G, Rasekh Sh, Diez JC. Preparation of high-performance $Ca_3Co_4O_9$ thermoelectric ceramics produced by a new two-step method. J Eur Ceram Soc 2013;33 (10):1747–54.

[41] Hammond CR. CRC Handbook of chemistry and physics, 90th ed. Boca Raton:CRC Press;2006.

[42] Woermann E, Muan A. Phase equilibria in the system CaO–cobalt oxide in air. J Inorg Nuc Chem 1970;32 (5):1455–59.

[43] Becherer G, Ifland R. Uber eine prazisionbestimmung der gitterkonstanten von silber nach dem ruckstrahlverfahren. Naturwissenschaften 1954;41:471-5.

[44] Mora M, Sotelo A, Amaveda H, Madre MA, Diez JC, Angurel LA, de la Fuente GF. Ag addition effect on laser textured Bi-2212 samples. Bol Soc Esp Ceram V 2005;44:199-203.

[45] Joo J, Singh JP, Warzynski T, Grow A, Poeppel RB. Role of silver addition on mechanical and superconducting properties of high-Tc superconductors. Appl Supercond 1994;2:401–10.

[46] Xiang P-H, Kinemuchi Y, Kaga H, Watari K. Fabrication and thermoelectric properties of $Ca_3Co_4O_9$/Ag composites. J Alloys Compd 2008;454:364-9.

Figure captions:

Figure 1. Powder X-ray diffraction patterns obtained for the $Ca_3Co_4O_9$ + x wt.% Ag samples; x = 0 (a); 1 (b); 3 (c); 5 (d); and 10 (e). The diffraction planes indicate the $Ca_3Co_4O_9$ phase and the # symbol identifies the (111) diffraction peak of Ag.

Figure 2. SEM micrographs performed on representative longitudinal polished surfaces of $Ca_3Co_4O_9$ + x wt.% Ag samples; x = 0 (a); 1 (b); 3 (c); 5 (d); and 10 (e). The Ag particles are indicated by arrows in (b) and the grey contrast matrix corresponds to the $Ca_3Co_4O_9$ phase. A higher magnification micrograph, performed in 3wt.% Ag samples, is illustrating the zones between the thermoelectric grains, where Ag is found (f).

Figure 3. SEM micrographs performed on representative longitudinal surfaces of $Ca_3Co_4O_9$ + x wt.% Ag samples; x = 0 (a); 1 (b); 3 (c); 5 (d); and 10 (e). Grey contrast is associated by EDS to the $Ca_3Co_4O_9$ phase and black one to porosity.

Figure 4. Flexural strength, together with its standard error bars, as a function of Ag content.

Figure 5. Temperature dependence of the electrical resistivity, as a function of Ag content, in $Ca_3Co_4O_9$ + x wt.% Ag samples, for x = 0 (●); 1 (■); 3 (▲); 5 (▼); and 10 (◆).

Figure 6. Temperature dependence of the Seebeck coefficient, as a function of Ag content, in $Ca_3Co_4O_9$ + x wt.% Ag samples, for x = 0 (●); 1 (■); 3 (▲); 5 (▼); and 10 (◆).

Figure 7. Temperature dependence of the power factor, as a function of Ag content, in $Ca_3Co_4O_9$ + x wt.% Ag samples, for x = 0 (●); 1 (■); 3 (▲); 5 (▼); and 10 (◆).

Table I. Cell parameters and volumes obtained with fullprof in samples with different Ag content

Sample (wt.%)	a	b	c	β	Volume
0 Ag	4.8423(4)	4.5698(6)	10.872(2)	98.20(1)	238.13(5)
1 Ag	4.8635(6)	4.5569(6)	10.851(1)	98.73(1)	237.69(5)
3 Ag	4.8634(4)	4.5573(5)	10.848(1)	98.66(1)	237.70(4)
5 Ag	4.8624(5)	4.5538(8)	10.833(1)	98.68(1)	237.13(6)
10 Ag	4.8569(1)	4.5521(9)	10.827(1)	98.60(1)	236.70(5)

Table II. Evolution of the mean densities, together with their standard error, and the % of the theoretical one, determined in the bulk $Ca_3Co_4O_9$ + xwt.% Ag samples.

x	Mean ρ (g/cm^3)	Std. error	% theor. ρ
0	3.75	0.02	80.2
1	4.11	0.03	87.4
3	4.19	0.03	88.0
5	4.32	0.02	89.9
10	4.48	0.02	90.5

Figure 1

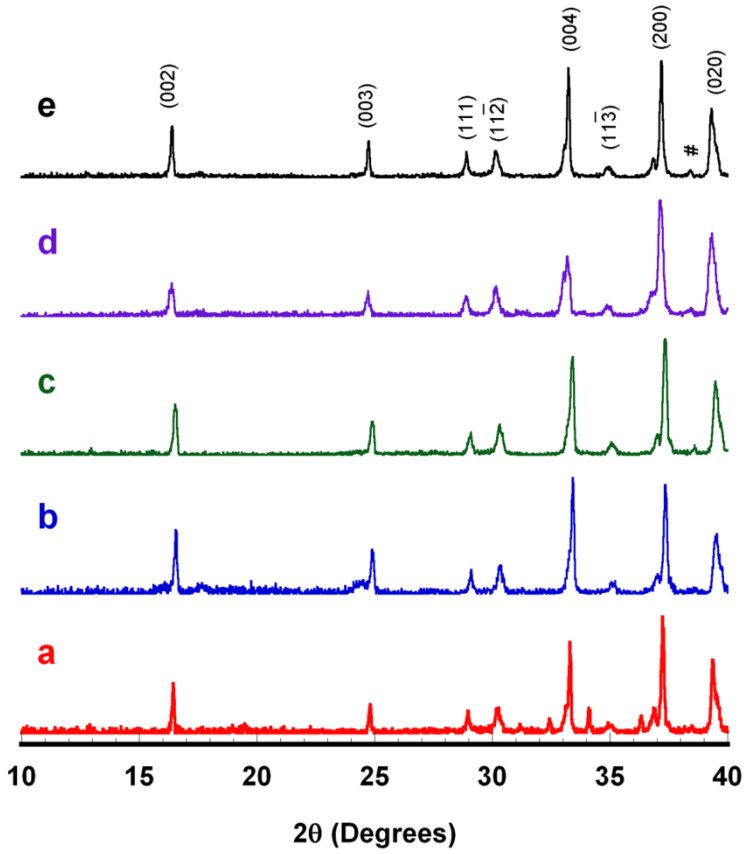
e
d
c
b
a
(002)
(003)
(111)
(11$\bar{2}$)
(004)
(11$\bar{3}$)
(200)
#
(020)
10
15
20
25
30
35
40
2θ (Degrees)

Figure 2

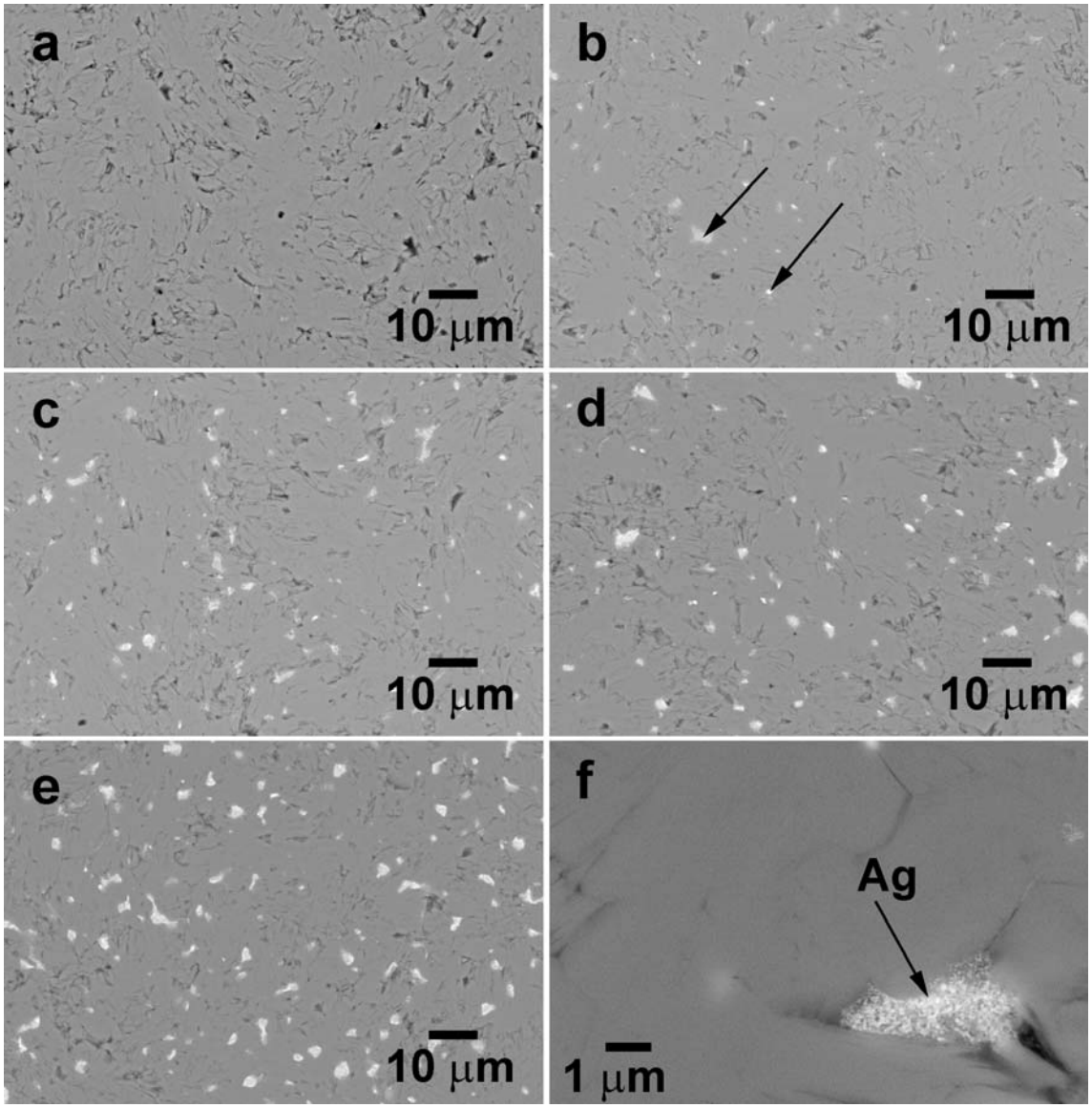

Figure 3

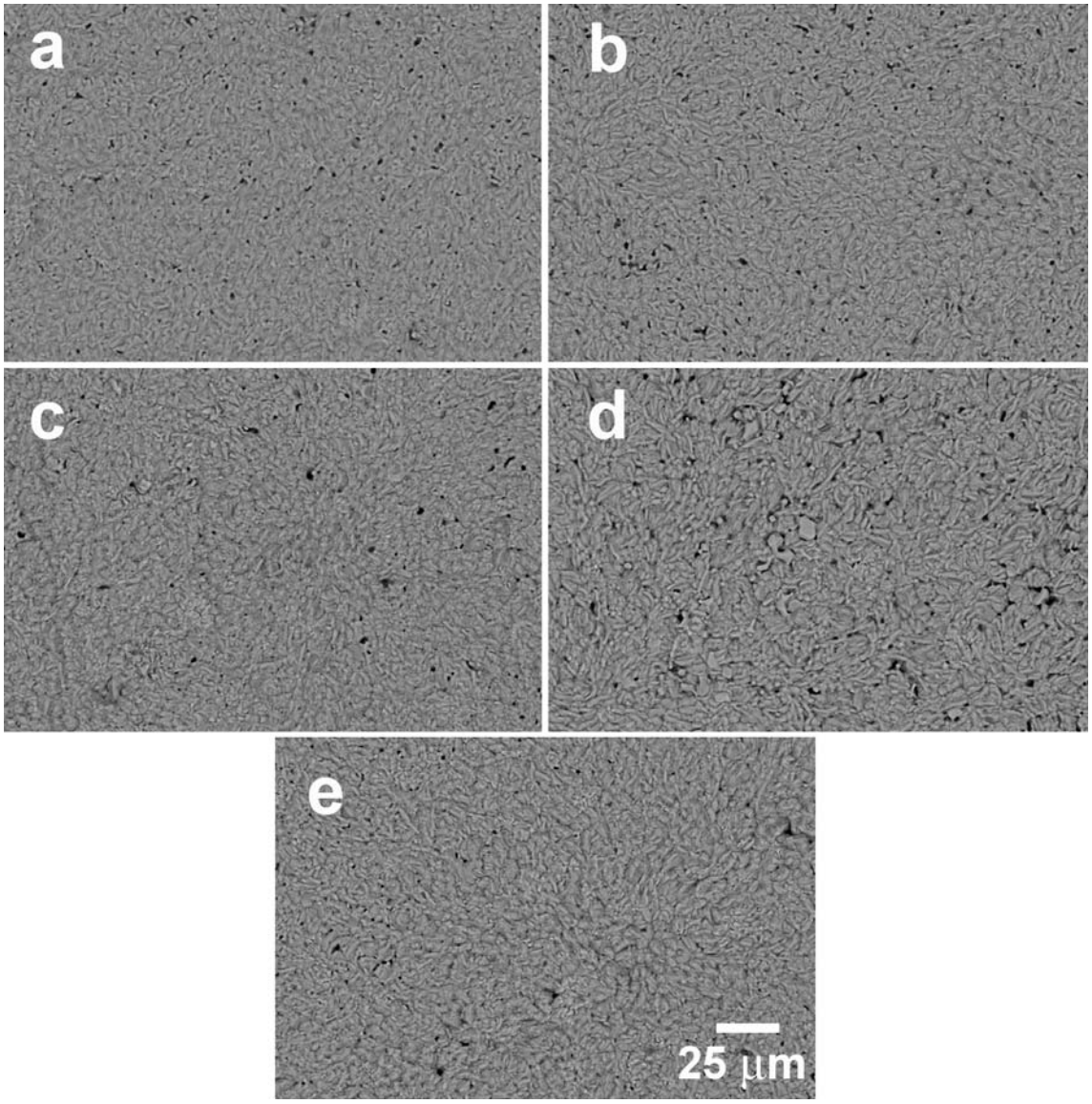

Figure 4

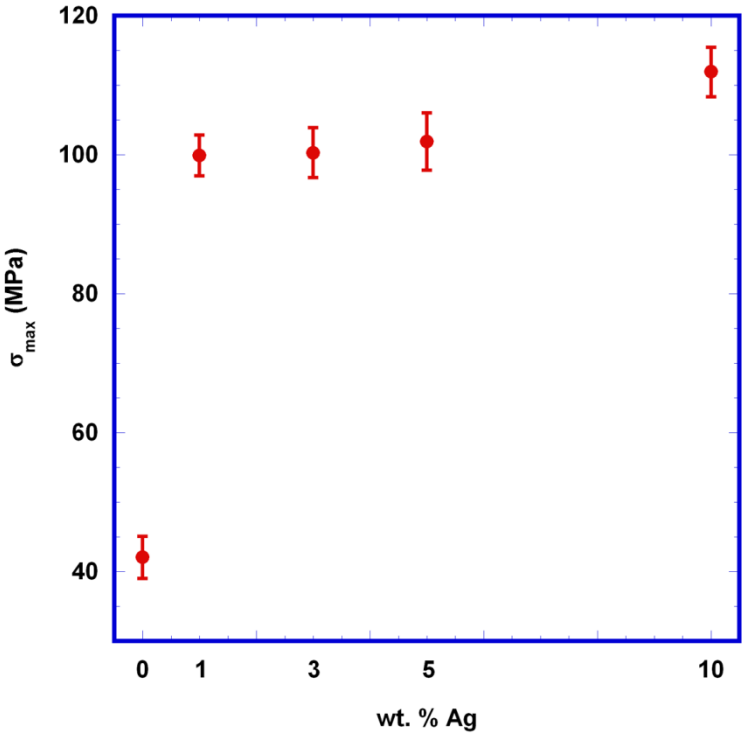

Figure 5

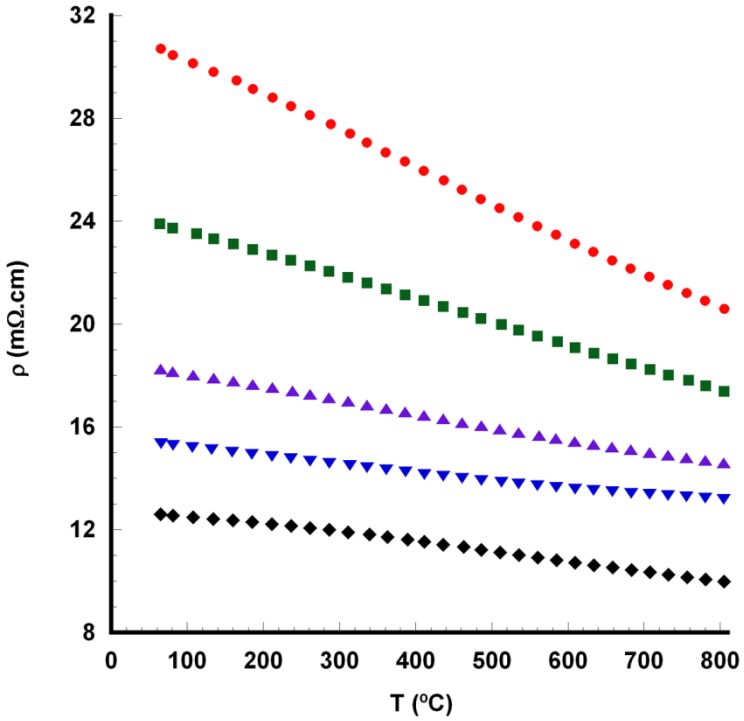

Figure 6

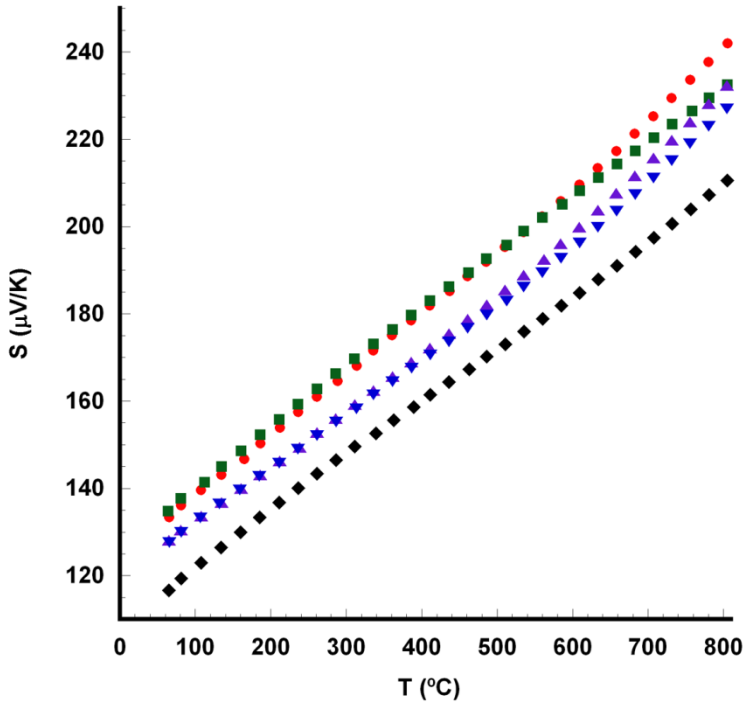
240
220
200
180
160
140
120
S (μV/K)
0
100
200
300
400
500
600
700
800
T (°C)

Figure 7

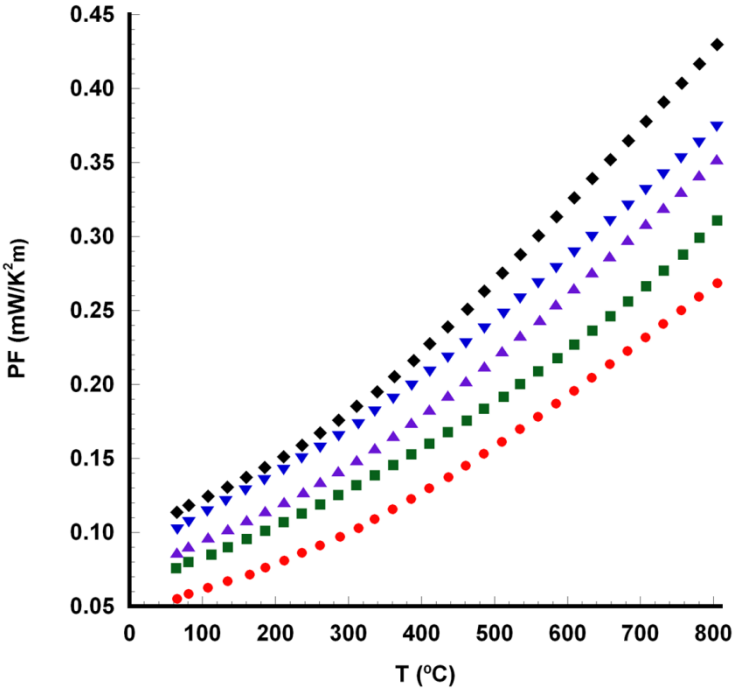
0.45
0.40
0.35
0.30
0.25
0.20
0.15
0.10
0.05
PF (mW/K²m)
0
100
200
300
400
500
600
700
800
T (°C)